11

Reverse-Engineering the Robustness of Mammalian Lungs

Michael Mayo[1], Peter Pfeifer[2] and Chen Hou[3]
[1]*Environmental Laboratory, US Army Engineer Research and Development Center, Vicksburg, MS*
[2]*Department of Physics, University of Missouri, Columbia, MO*
[3]*Department of Biological Sciences, Missouri University of Science and Technology, Rolla, MO, USA*

1. Introduction

This chapter is devoted to reverse-engineering the cause of a dramatic increase in the total oxygen uptake rate by the lung, wherein oxygen is supplied to the blood to meet the increasing energetic demands between rest and exercise. This uptake rate increases despite a much smaller increase in the oxygen partial pressure difference across the lung's exchange tissues (e.g. alveolar membranes), thought to mainly drive the oxygen-blood transfer in a similar way that electric currents are driven by voltage differences according to Ohm's law. As we explain below, a full understanding of this special property has the potential to improve various engineering processes, such as stabilizing chemical yields in heterogeneous catalysis, improving the efficiency of heat-transporters, and improving energy generation in electrochemical reactors.

To reverse-engineer the cause of this mostly pressure-independent increase in the oxygen uptake rate, we focus on the development of mathematical models based on the rate-limiting physical transport processes of i) diffusion through the airway spaces, and ii) "reaction" of the oxygen molecules across the surface of permeable membranes responsible for transferring oxygen from air to blood. Two of these mathematical models treat the terminal, or acinar, airways of mammalian lungs as hierarchical trees; another treats the entire permeable surface as fractal. By understanding how the parameters of these mathematical models restrict the overall oxygen uptake rate, we infer how the lung preserves its function when exposed to environmental hazards (e.g. smoking), damage (e.g. surgery), or disease (e.g. emphysema). The focus of our work here is to discover, or reverse engineer, the operational principles that allow mammalian lungs to match increased oxygen demands with supply without any significant alteration of its "hardware."

We first begin with a mathematical description of oxygen diffusion as the primary transport mechanism throughout the airways responsible for the oxygen uptake in the deep regions of the mammalian lungs studied here. We then discuss several different, but complementary analytical models that approach the oxygen-transport problem from different directions, while also developing a new one. Although these models are different from one another

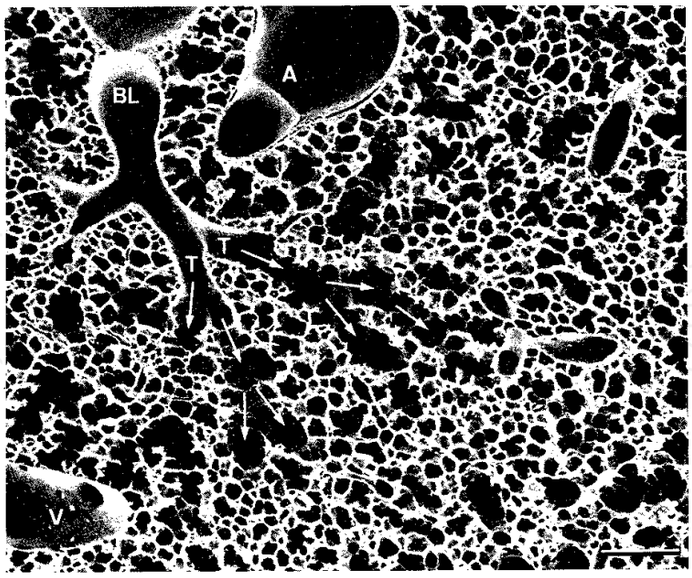

Fig. 1. Scanning electron micrograph of the perfusion-fixed lung tissue (Weibel, 1984), showing transition between peripheral bronchiole (BL) and terminal bronchiole (T). Alveolar ducts are denoted by arrows in the direction of downstream flow, near pulmonary arteries (A) and veins (V). Scale marker is 200 μm.

in how they treat the exchange-surface, they all consistently predict a region of the parameter space in which the current is "robust;" i.e. changes or error in the parameters do not affect the functional state of the system. Finally, we apply physiological data for the human lung–the prototypical mammalian lung studied here–to validate these models against experimental measurements; we use them as a tool to reverse-engineer how the human lung supplies the body with increasing oxygen currents under the body's increasing oxygen demands that occur, for example, during heavy exercise.

2. Motivation

Mammalian lungs regulate the exchange of respiratory gases (here we focus on molecular oxygen, O_2) between air and pulmonary blood, delivering oxygen to cells that use it to drive energy metabolism, such as glycolysis. Beginning from the trachea, these gases are transported downstream throughout the bronchial tree by convection until their speed drops drops below the local diffusion speed, wherein further transport toward the periphery of the lung occurs by stationary diffusion. As shown in Fig. 1, the airways in which this transition occurs, termed the transitional bronchioles, are defined by the appearance of air sacs, or alveoli, that appear along the walls of the airway channels, termed acinar ducts (Weibel, 1984). While only sparsely populating the walls of the transitional bronchioles, these alveoli dominate the walls of the acinar airways, which lay only a few branch generations downstream of the transitional bronchioles. The epithelial cells lining the alveoli are tightly packed, so they form a jointless surface of alveolar membranes across which the gas exchange almost entirely occurs (Weibel, 1984).

The oxygen uptake rate, I, measured in units of moles of gas transferred across the entire surface of alveolar membranes of the lung per unit time, measures the ability of the body to

meet the changing energetic demands of its tissues under changing physiological conditions, such as foraging or predation. For example, altering cell metabolism increases/decreases oxygen demands (as a vital component in glycolysis), and the mammalian lung, as a whole, responds by automatically increasing/decreasing this current without invoking any biochemical feedback loops.

There are several steps between oxygen in the air and its final delivery to the cell. The rate-limiting step is its diffusion to, and across, the surface of alveolar membranes that collectively serve as the gas-exchange surface. It then binds with the erythrocytes, or red blood cells in the pulmonary arteries, to any of the four binding sites on hemoglobin, which allows for its dissolution in blood plasma. An oxygen partial pressure difference between air, p_a, and erythrocytes, p_e, serves as the driving force in the oxygen uptake rate across the membranes, and can be written as (Comroe, 1962; Weibel, 1984):

$$I = T_{lung} \left(p_a - p_e \right), \tag{1}$$

wherein T_{lung} is the total diffusing capacity of the mammalian lung (in units of oxygen molecules transferred to erythrocyte per unit time and pressure). Because diffusing oxygen moves first across a barrier of alveolar membranes and then through the blood plasma, they can be viewed as resistors connected in series (Hou et al., 2010), in which the same current flows through each biological "resistor." Equation 1 can then be rewritten in terms of only the oxygen partial pressure difference across the membranes alone, $p_a - p_b$ (Weibel, 1984):

$$I = T_m \left(p_a - p_b \right), \tag{2}$$

wherein T_m is the membrane's diffusing capacity for oxygen.

As the body increasingly demands more oxygen to supply muscles and other tissues with chemical energy, the uptake rate, as given by Eqn. 2, increases 20-fold under the most strenuous exercise and breathing conditions as compared to the resting state, although the driver of the oxygen current–the partial pressure difference–increases only 2–fold under these same conditions (Weibel, 1992). The diffusing capacity of the membranes is, T_m, therefore, is almost entirely responsible for this increase in oxygen uptake rate; not the partial pressure difference.

To put this result in perspective, consider an analogy between electrical and biological circuits, wherein biological surface areas and permeabilities play the role of electrical impedance, chemical/nutrient exchange and uptake rates across these biological surfaces (e.g. oxygen uptake rates) play the role of electric currents, and partial pressure differences across biological surfaces play the role of voltage differences across electrical components. Relationships of the type given by Eqn. 2 are therefore analogous to Ohm's law in electric circuits. To say that the oxygen partial pressure difference does not, in effect, provide for the entirety of the observed increase in oxygen current supplied to the body by the lung, is equivalent to stating that a voltage difference is not entirely responsible for increasing the electrical current through a circuit's component, such as a resistor. Here we use mathematical modeling to explain this phenomenon, and use it to determine the cause of the lung's robustness–it's ability to provide a constant oxygen current to the blood despite disease or damage to its exchange tissues.

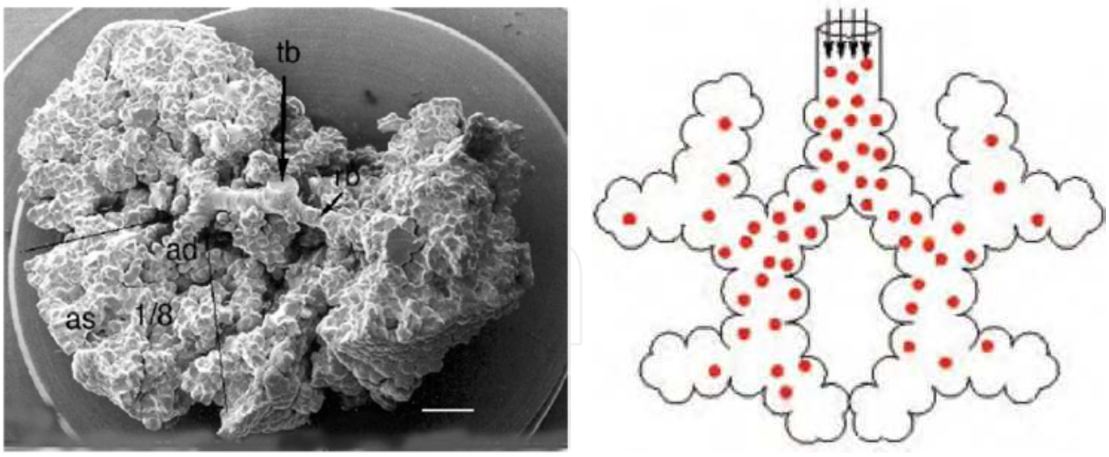

(a) (b)

Fig. 2. (a) Silicon rubber case of a rabbit lung acinus (Sapoval et al., 2002); (b) illustration of a model mammalian lung acinus, wherein oxygen (red) concentration gradients are established by limited access to the acinar volume by by diffusion throughout the airways (Sapoval et al., 2002).

3. Mathematical modeling of mammalian lungs

3.1 Transitions between rest and exercise determine the size of the physiological diffusion space

Oxygen uptake in mammalian lungs occurs across the alveolar ducts of the acinar airways–the elementary gas exchange unit of mammalian lungs–which host the alveoli (Weibel, 1984), as illustrated in Figs. 1 and 2. These are the airways in which oxygen is transported entirely by diffusion in the resting state, and there are $\sim 10^5$ of them in human lungs under these conditions (Hou et al., 2010). The branching generation at which the tracheobronchial tree ends defines the entrance to the acinar airways, and is marked by the convection-diffusion transition in the resting state, which can be located through mass-balance considerations.

The mass flow-rate through a duct of the ith generation of bronchial tree, $\dot{M} = \rho v_i A_i$ (in units of mass per time), is written in terms of the cross-sectional area of the duct, $A_i = \pi r_i^2$, the speed of the gases across this area, v_i and the local oxygen density, ρ. No molecules of the gas is lost across a branching point, the point in which a parent duct extends into m-many daughter ones, because there are no alveoli lining them. Mass-balance in this branch gives $\dot{M}_i = m\dot{M}_{i+1}$, so that the transport speed can be written in terms of its speed at the trachea, v_0:

$$v_i = \frac{v_0}{\sum_{j=0}^{i} m^{j/3}} = \frac{m-1}{m^{(i+1)/3}} v_0. \tag{3}$$

Here, we have applied Murray's law for the bronchial tree, $r_i = r_0 m^{-i/3}$ (Weibel, 1984), connecting radii of downstream branches, r_i, to that of the trachea, r_0. Note that $m = 2$ for mammalian lungs. The tree's total cross-sectional area therefore increases exponentially with branching generation according to Eqn. 3, resulting in a drastic decrease of the oxygen velocity within the deeper airway branches as compared to the trachea.

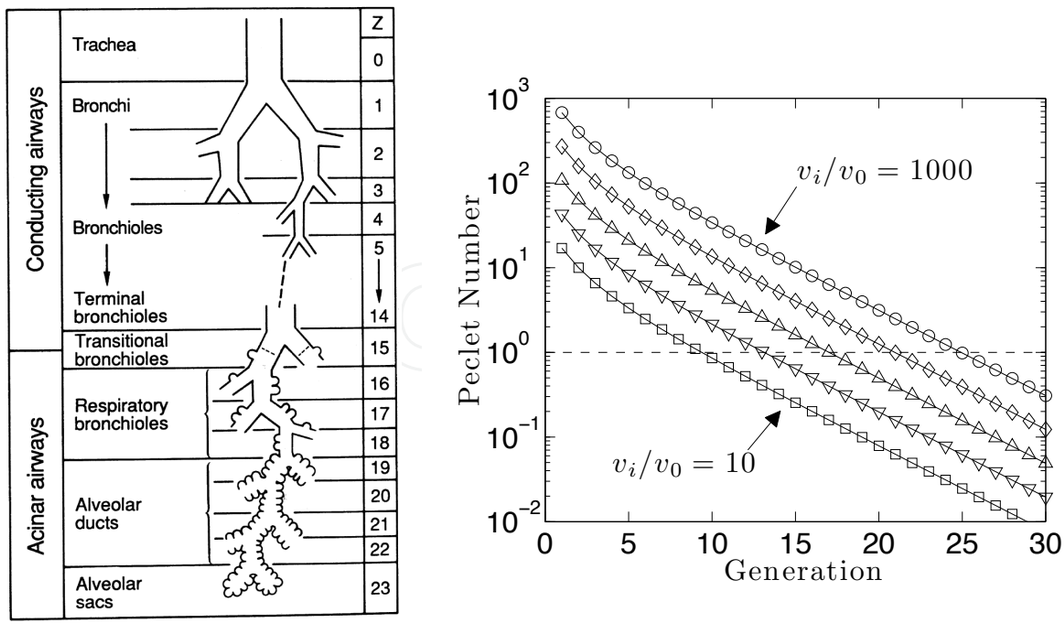

(a) (b)

Fig. 3. (a) Branching hierarchy of mammalian lungs (Weibel, 1984); (b)Velocity of respiratory gases, such as molecular oxygen, decrease with increasing depth into the bronchial tree. The convection-diffusion transition occurs when these gas velocities fall below the local diffusion speed.

The Peclet number gives the ratio of diffusive to convective flow rate, and the branching generation at which the Peclet number equals 1 gives the convection-diffusion transition. In the human lung, for example, this transition occurs at approximately the 18th branching generation in the resting state (Hou 2005; Hou et al., 2010). The airway "unit" defined by the remaining five generations are termed a 1/8 subacinus (Haefeli-Bleuer and Weibel, 1988). For different exercise states, however, this transition occurs deeper than generation 18, because the inspiration speed at the trachea increases. This effect is illustrated in Fig. 3 by evaluating Eqn. 3 for varying speeds at the trachea in units of the diffusional speed of oxygen in air.

In reality, transitions between exercise conditions is smooth; however, in light of Fig. 3, we refer herein to an "exercise state" in terms of how the exercise conditions affect the lung's convection-diffusion transition. In this context, four distinct exercise states can be identified in humans (Sapoval et al., 2002; Felici et al., 2004; Grebenkov et al., 2005; Hou 2005; Hou et al., 2010), which serve as the exemplary mammalian lung system for remainder of this article. These regimes are *rest* ($i = 18$), *moderate exercise* ($i = 19$), *heavy exercise* ($i = 20$), and *maximum exercise* ($i = 21$). On average, the human lung terminates with a total depth of 23 branching generations, giving an approximately equal length to all downstream branching paths. In terms of subacinar trees, these exercise states can be associated to airways of depth $n = 23 - 18 = 5$ (rest), $n = 23 - 19 = 4$ (moderate exercise), $n = 23 - 20 = 3$ (heavy exercise), and $n = 23 - 21 = 2$ (maximum exercise) (Hou et al., 2010).

The subacinar trees identified in terms of these four discrete "exercise states," define the corresponding diffusion space relevant for each breathing regime. Because diffusion occurs at rest in the network of alveolar ducts, rather than the respiratory bronchioles, we

consider an elementary airway unit to be a "1/8 subacinus" (Weibel, 1984) that begins with branching generation 18, instead of an entire lung acinus that includes respiratory bronchioles, and supports a network of alveolar ducts spanning 5 generations. Successive subacinii corresponding to the other exercise states are termed 1/16- (moderate exercise), 1/32- (heavy exercise), and 1/64-subacinii (maximum exercise).

3.2 Equations for oxygen transport throughout and across the acinar tree

While strenuous exercise pushes the diffusion source deeper into the lung, as evidenced by Eqn. 3 and Fig. 3, the evolution of the oxygen concentration difference between the subacini entrance and the blood side of the membranes, $c(\mathbf{x})$, obeys the stationary diffusion equation (Felici et al., 2003):

$$\nabla^2 c(\mathbf{x}) = 0, \text{ with } \mathbf{x} \in \text{diffusion space.} \tag{4}$$

The concentration across the tree's entrance (the diffusional "source") gives the first boundary condition,

$$c(\mathbf{x}) = c_a, \text{ with } \mathbf{x} \in \text{source.} \tag{5}$$

The oxygen flux entering the gas-exchange (the diffusional "receptor") surface is matched with the flux moving through it (Hou, 2005):

$$\nabla c(\mathbf{x}) \cdot \mathbf{n}(\mathbf{x}) = \frac{c(\mathbf{x}) - c_b\beta_a/\beta_b}{\Lambda}, \text{ with } \mathbf{x} \in \text{boundary,} \tag{6}$$

wherein the β_a and β_b are the solubility of oxygen in air and blood, respectively.

The parameter $\Lambda = D_a/W$ is the ratio of the diffusivity of oxygen in air, D_a, to the surface permeability, W, has units of length, and is the only length scale for the boundary-valued problem defined by Eqns. 4 to 6. Moreover, it has an elegant physical interpretation: it measures the length along the surface a diffusing molecule visits before it is absorbed by the surface, and for this reason is termed the exploration length (Pfeifer & Sapoval, 1995).

3.3 The effective surface area: area of the active zones involved in the oxygen transport

Although the diffusion-reaction problem defined by Eqns. 4 to 6 give concentrations across the tree's exchange surface, we are instead interested in the *total* current of molecules supplied to the blood by the whole of the airway tree. Computing this current for a single subacinus, I_g, from Eqns. 4 to 6 can be carried out by integrating the concentrations over its entire surface, S_g (Hou et al., 2010):

$$I_g = W \int_{\mathbf{x}\in S_g} \left(c(\mathbf{x}) - c_b\beta_a/\beta_b\right) dS \tag{7}$$

Manipulating this equation leads to an expression for the current in terms of a constant concentration difference:

$$I_g = W S_{eff,g} \left(c_a - c_b\beta_a/\beta_b\right), \tag{8}$$

wherein $S_{eff,g}$ is a function of the exploration length (Hou, 2005):

$$S_{eff,g}(\Lambda) = \int_{\mathbf{x}\in S_g} \frac{c(\mathbf{x};\Lambda) - c_b\beta_a/\beta_b}{c_a - c_b\beta_a/\beta_b} dS. \tag{9}$$

This quantity, termed the effective surface area (Felici et al., 2003; Felici et al., 2004; Grebenkov et al., 2005; Hou, 2005; Hou et al., 2010), measures the "active" portion of the tree's surface, and is generally less than its total, i.e. $S_{eff,g} \leq S_g$. The difference in these areas is unused in any molecular transport, and is "inactive," or *screened* from molecular access to it.

This screening can be conceptualized in terms of the exploration length (see below). For example, $\Lambda = 0$ (i.e. permeability is infinite) describes a situation in which no molecules explore areas of the tree beyond the entrance, being immediately absorbed by the surface on their first contact with it. This regime is termed *complete screening*. In contrast, $\Lambda = \infty$ (i.e. permeability is zero) implies that oxygen molecule hits the surface many times and eventually visits the entire surface, marking the regime of *no screening*. These facts provide a powerful conceptual picture of the lung's operational principles: to increase the current under constant conditions of membrane permeability and concentration difference, the effective surface area must increase proportionally. So, for breathing/exercise states of increasing exercise intensity, ever larger fractions of the lung's exchange area must be recruited for the molecular transport across it.

3.4 Total current into the tree

The current crossing the lung's exchange areas is the sum of currents contributed from each individual branch of the subacinar tree, given by Eqn. 8:

$$I = \sum_{i=1}^{N_g} I_{g,i}, \tag{10}$$

wherein N_g gives the number of gas exchangers in the lung in the current exercise state (explained below). Taking an average of both sides of Eqn. 10 over all such gas-exchangers gives $I = N_g I_g$, wherein I_g is the average current supplied by a single subacinus. The total current can then be written as

$$I = N_g W S_{eff,g} \left(c_a - c_b/\beta_a/\beta_b\right). \tag{11}$$

This equation, Eqn. 11, can be rewritten in terms of the physiological variables of Eqn. 2:

$$I = \frac{D_m \beta_m S_{eff}}{\tau} \left(p_a - p_b\right) = W S_{eff} \left(c_a - c_b \beta_b/\beta_a\right), \tag{12}$$

wherein the diffusing capacity of the lung has been replaced by the diffusion coefficient of oxygen through the surface of alveolar membranes, D_m, the thickness of the membrane-barrier, τ, the solubility of oxygen in the membranes, β_m , and the effective surface area of the entire lung, S_{eff}. The permeability can itself be expressed in terms of measurable quantities, and dependent upon the thickness of the membranes:

$$W = \frac{D_m \beta_m}{\tau}. \tag{13}$$

To good approximation, the thickness of the membranes is constant and the permeability is position-independent.

The total current, Eqn. 11, crucially depends on how the effective surface area responds to the current physiological conditions. Integrating directly from the concentrations, as in Eqn. 9, requires a solution to the difficult boundary-valued diffusion-reaction problem defined above (Eqns. 4 to 6). In the next section, we review an entirely geometrical method, termed the Rope-Walk Algorithm, permitting us to side-step the difficult integration required by equation 9, and, through Eqn. 11, allows for a solution of Eqns. 4 to 6 to be found without directly solving the full diffusion-reaction problem.

3.5 Rope-Walk algorithm: solving the diffusion equation without solving the diffusion equation

We consider a self-similar surface with fractal dimension D_f, surface area S, and composed of cubic elementary units of side length, l, which serves as a molecular "receptor" in the diffusion-reaction problem. Molecules encounter this surface after diffusing from the source with area S_s, which is much smaller than the receptor's total surface area $S_s << S$. Only surface sites that such diffusing molecules visit while "walking" along it, even if the exploration length is zero, are considered here. Such sites are very close to the diffusion source. A rope of length Λ is rolled out along the surface as diffusing molecules "walk" along it, which determines the diameter of the profile so covered/explored by ropes, from which the effective surface area explored by diffusing molecules is found, S_{eff} (Hou, 2005; Hou et al., 2010):

$$S_{eff} = \begin{cases} S_s & \Lambda < l \\ S_s \left(\Lambda/l\right)^{\left(D_f-2\right)/\left(D_f-1\right)} & l \leq \Lambda \leq l \left(S_s^{1/2}/l\right)^{D_f-1} \\ S_s^{1/2}\Lambda & l \left(S_s^{1/2}/l\right)^{D_f-1} \leq \Lambda \leq S_s^{1/2} S \\ S & S_s^{1/2} S \leq \Lambda \end{cases}, \tag{14}$$

describing four screening regimes, respectively given as: *complete screening*, *strong partial screening*, *weak partial screening*, and *no screening*.

These ropes decompose the total surface into regions accessible to the diffusing molecule, and regions inaccessible, which are determined by how the rope length compares with other three length scales: side lengths of the elementary unit, the size of the diffusion source, and the "perimeter" of the membrane surface. If the rope length is smaller than an elementary block unit, $\Lambda < l$, then only the region very close to the source, with area S_s, is active in transport, which marks the regime of complete screening. If the rope is longer than the perimeter of the surface profile, then molecules explore the entire surface before they cross it, and this is the case of no screening. In between, there are two partial screening cases, in which the rope is longer than the elementary block but not long enough to wrap the whole surface.

4. Mathematical models of gas-exchangers

Several mathematical models describing molecular transport across reactive surfaces have been used to study the response of the oxygen current across mammalian lungs at physiological conditions (Hou et al., 2010; Mayo, 2009; Grebenkov et al., 2005). Although each model treats the exchange surface differently, they each provide similar predictions of, and independently verify, the "robustness" of the human lung (described below). More importantly, these models provide fully analytic formulas of the total current, allowing for transparent relationships to be derived between this robustness and the model's parameters.

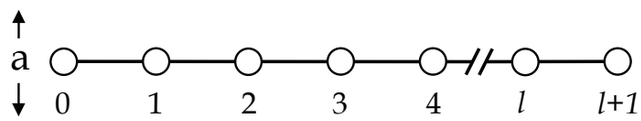

Fig. 4. Discretized branch of an alveolar duct in the square-channel model.

Together with Eqn. 11, the Rope-Walk algorithm serves as the first of three predictive mathematical models we describe here. The next model is the square-channel model proposed by Grebenkov and his collaborators (Grebenkov et al., 2005). The third model, the Cayley tree model, is a new model of the acinar tree we present here.

4.1 Square-channel model

4.1.1 Modeling a single alveolar duct

In an approach developed by Grebenkov and his collaborators (Grebenknov et al., 2005), a single branch of the subacinar tree is modeled discretely, as a square channel, from which the entire acinar tree is assembled. Figure 4 illustrates a single branch in this model, wherein oxygen molecules diffuse throughout a channel of $d = 3$ dimensions. These molecules begin diffusion from a square cross-section of area a^2 to ultimately "react" with the exchange surface along the channel walls, which occurs at discrete intervals separated by a distance a.

The full diffusion-reaction problem is therefore mapped onto a discrete, one-dimensional process that evolves according to the following diffusion "rules" (Grebenkov et al., 2005). Molecules currently at site i move to the left (site $i-1$) or right (site $i+1$) with probability $1/2d$, or stay on the current site with probability $(1-\sigma)(1-1/d)$, wherein $\sigma = 1/(1+\Lambda/a)$ is the absorption probability of the molecule with the surface. Finally, the molecule crosses the surface with probability $\sigma(1-1/d)$. Collectively, these rules can be written as a finite difference equation (Grebenkov et al., 2005), which is a discretized version of Eqns. 4 to 6:

$$\frac{1}{2}\left(c_{i-1}+c_{i+1}\right)-c_i=\sigma\left(d-1\right)c_i, \tag{15}$$

wherein $i = 0, 1, \ldots, l$.

Equation 15 can be solved by applying the discrete Fourier transform, with boundary conditions $c_0 = c_{ent}$ and $c_{l+1} = c_{ext}$ (Grebenkov et al., 2005). These solutions can be expressed in terms of linear relationships between concentrations at lattice sites 0,1,l, and $l+1$, shown in Fig. 4:

$$c_1=\left(1-u_{\sigma,k}\right)c_{ent}+\nu_{\sigma,k}c_{ext}, \text{ and} \tag{16}$$

$$c_k=\nu_{\sigma,k}c_{ent}+\left(1-u_{\sigma,k}\right)c_{ext}. \tag{17}$$

Here, the coefficients $u_{\sigma,k}$ and $\nu_{\sigma,k}$ depend only on the dimension of the diffusion space, d, and the absorption probability, σ (Grebenkov et al., 2005):

$$u_{\sigma,k}=1-\frac{s_{\sigma,k}}{\left([1+(d+1)\sigma]s_{\sigma,k}+1/2\right)^2-s_{\sigma,k}^2}, \text{ and} \tag{18}$$

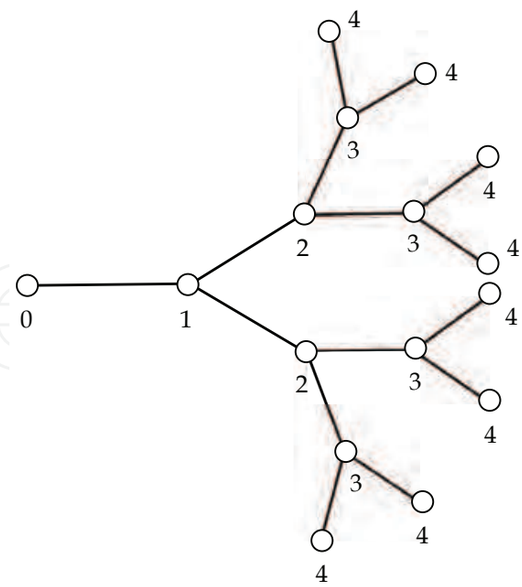

Fig. 5. Exemplary hierarchical bifurcating tree of depth $n = 3$.

$$\nu_{\sigma,k} = 1 - \frac{[1 + (d+1)\,\sigma]s_{\sigma,k} + 1/2}{\left([1 + (d+1)\,\sigma]s_{\sigma,k} + 1/2\right)^2 - s_{\sigma,k}^2}, \tag{19}$$

wherein the sum, $s_{\sigma,k}$, is given by

$$s_{\sigma,k} = \frac{1}{2k}\sum_{j=0}^{k-1}[1 + (d-1)\,\sigma - cos\,(2\pi j/k)]^{-1}. \tag{20}$$

Equations 16 through 20 give the concentrations in a single duct near its ends. In the following sections this result is extended to describe the oxygen currents crossing the exchange surface of alveolar membranes lining these ducts.

4.1.2 Building the tree from a single branch

A treelike structure can be assembled from the individually modeled branches of the previous section, and Fig. 5 illustrates of an exemplary bifurcating tree. Its branching hierarchy is conceptualized by parent and daughter branches, in which m-many daughter branches extend from each parent branch at the branch points. In this model, the branches are subscripted according to whether they are an entrance or exit quantity of a branch in a given generation, i.e. $c_{ent,i}$ is the entrance concentration of a branch in the ith generation along any path from leaf to root. The problem, then, is to compute the current, I, leaving the surface of the entire tree, which is the sum of the contributions from each individual branch, $I_i = I_{ent,i} - I_{ext,i}$:

$$I = \sum_{k=0}^{n} m^k \left(I_{ent,k} - I_{ext,k}\right) + m^n I_{ext,n} = I_{ent,0}, \tag{21}$$

wherein we have used $I_{ext,k-1} = mI_{end,k}$. From Eqn. 21, we only need compute the current entering the tree by its root to find the current leaving the effective area of the reactive surface. A branch-by-branch renormalization procedure is now used to calculate this quantity.

4.1.3 Branch-by-branch calculation of the total current into the tree

The currents entering and leaving any branch of the tree can be written in terms of concentrations there (Grebenkov et al., 2005):

$$I_{ent} = DS_0 \frac{c_0 - c_1}{a}, \text{ and } I_{ext} = DS_0 \frac{c_l - c_{l+1}}{a}, \tag{22}$$

wherein $S_0 = a^{d-1}$ is the area of a square cross-section for the channel. Applying these expressions to Eqns. 16 and 17 relates the entrance and exit currents with their respective concentrations (Grebenkov et al., 2005):

$$c_{ent} = \frac{u_{\sigma,l}}{v_{\sigma,l}} c_{ext} + \frac{a}{DS_0 v_{\sigma,l}} I_{ext}, \text{ and } I_{ent} = \frac{u_{\sigma,l}}{v_{\sigma,l}} I_{ext} + \frac{DS_0}{a} \frac{u_{\sigma,l}^2 - v_{\sigma,l}^2}{v_{\sigma,l}} c_{ext}. \tag{23}$$

Beginning with a terminal branch, the current leaving its end cross-section can be written in terms of the exploration length (Grebenkov et al., 2005):

$$I_{ext,n} = \frac{DS_0}{\Lambda} c_{ext,n}, \tag{24}$$

allowing for the current entering the branch to be given by

$$I_{ent,n} = DS_0 \frac{(\Lambda/a)\left[u_{\sigma,l}^2 - v_{\sigma,l}^2\right]}{\Lambda u_{\sigma,l} + a} c_{ent,n}. \tag{25}$$

Since a terminal branch is the daughter branch to one in the $n-1$ generation, and noting both mass conservation at the branch point, $I_{ext,n-1} = mI_{ent,n}$, and that concentrations are independent of the labeling there, $c_{ext,n-1} = c_{ent,n}$, we find that

$$I_{ext,n-1} = \frac{DS_0}{f(\Lambda)} c_{ext,n-1}, \tag{26}$$

wherein

$$f(\Lambda) = \frac{a}{m} \left(\frac{(\Lambda/a)\, u_{\sigma,l} + 1}{(\Lambda/a)\left(u_{\sigma,l}^2 - v_{\sigma,l}^2\right) u_{\sigma,l}} \right). \tag{27}$$

Comparing Eqns. 26 to 27 to Eqn. 24, it is clear that the current leaving a branch in the $n-1$ generation can be viewed as a boundary condition across the leaves of a "reduced" tree of depth $n-2$. This procedure can be continued until the current entering the tree by its root is expressed in terms of the concentration there, c_0 (Grebenkov et al., 2005):

$$I = \frac{DS_0}{mf^{n+1}(\Lambda)} c_0, \tag{28}$$

wherein $f^{n+1}(\Lambda) = f \circ \cdots \circ f(\Lambda)$ gives the $n+1$–fold functional composition of Eqn. 27, and, with $d = 3$, $S_0 = a^2$ is the cross-section of the square channel.

4.2 Cayley tree model

Instead of modeling an acinus as a hierarchical tree of square channels, here we consider these branches as cylinders; this symmetry allows for a continuous description of the concentrations along its branches (Mayo 2009; Mayo et al., 2011). This model is flexible enough to include scaling relationships between parent and daughter branches, giving the total current in terms of the tree's fractal dimension.

4.2.1 Scaling relationships and fractal dimensions of the fractal Cayley tree

To account for scaling between the tree's branches, we adopt the following labeling scheme. The width and length of each branch is given by $2r_{e_i}$ and L_{e_i}, respectively, wherein $e_i = (i, i+1)$ label the edges of the Cayley graph in terms of its node, as illustrated by Fig. 5, and $i = 0, 1, \ldots, n, n+1$, with n being the depth of the tree. The single entrance branch, $e_0 = (0, 1)$, is termed the "trunk," whereas the m^n-many terminal branches, each labeled by $e_n = (n, n+1)$, are those composing its canopy, or "leaves."

We decompose the tree's surface into two parts: i) the canopy, or the surface composed of the union of end-caps of the terminal branches, and ii) the tree's cumulative surface area, or the sum of all surfaces minus the end cross-sections. The width and length of daughter branches can be expressed in terms of the those quantities for the parent branch through scaling relationships for their length, $m\left(L_{e_i}\right)^{D_{tree}} = L_{e_{i-1}}^{D_{tree}}$ and width, $m\left(r_{e_i}\right)^{D_{canopy}} = r_{e_{i-1}}^{D_{canopy}}$ (Mandelbrot, 1982). The ratios of these quantities across successive generations can be expressed in terms of the scaling exponents for the cumulative surface of the tree, D_{tree} , and its canopy, D_{canopy}:

$$p = m^{-1/D_{tree}}, \text{ and } q = m^{-1/D_{canopy}}. \tag{29}$$

For simplicity, we assume the length and width of branches in the same generation are of equal length and width; however, we allow branches to scale in width or length across generations: $p = p_{e_i} = L_{e_i}/L_{e_{i+1}}$ and $q = q_{e_i} = r_{e_i}/r_{e_{i+1}}$ for $i = 0, 1, \ldots, n-1$. These scaling exponents can be equated with the fractal dimension of the tree's cumulative and canopy surface areas (Mandelbrot, 1982; Mayo, 2009).

4.2.2 Helmholtz approximation of the full diffusion-reaction problem in a single branch

For cylindrical branches in which the ratio of radius to length, termed the aspect ratio, r/L, is "small," the oxygen concentration is, to very good approximation, dependent only on the variable describing its axis, x (Mayo, 2009). Mass-balance of the oxygen flux in the cylinder gives a Helmholtz-style equation for the concentration in the tube (Mayo et al., 2011):

$$\frac{d^2}{dx^2} c\left(x\right) - \left(\frac{\phi}{L}\right)^2 c\left(x\right) = 0. \tag{30}$$

wherein the Thiele modulus of the branch is given in terms of the exploration length:

$$\phi = L\sqrt{\frac{2}{r\Lambda}}. \tag{31}$$

The tree is composed of three classes of branches, each defined by type of boundary condition given across the beginning and end of the tube. Giving an exit concentration (written in terms

of the exit current) and an entrance current for a terminal branch, $c(x = L) = I_{ext}/W\pi r^2$ and $d/dxc(x = 0) = -I_{ent}/D\pi r^2$, gives a solution to Eqn. 30 connecting the entrance and exit currents (Mayo, 2009):

$$c(x) = \frac{I_{ent}\sinh[\phi(1 - x/L)] + I_{ext}\phi\cosh(\phi x/L)}{(\pi\rho^2 D/L)\,\phi\cosh\phi}. \tag{32}$$

Similar equations can be found for the trunk and "intermediate branches," resulting in equations that link entrance and exit concentrations, or a mixture of concentrations and currents (Mayo et al., 2011). These equations are used in a renormalization calculation, similar to the branch-by-branch calculation of the square-channel model above, to compute the total current entering the tree by its root.

4.2.3 Total current into the tree

Elsewhere we demonstrate how equations of the type described by Eqn. 32 can be employed for a branch-by-branch calculation of the total current, similar to that of the square-channel model described above, and written in terms of the scaling ratios of Eqn. 29 (Mayo et al., 2011). This calculation results in

$$I = \frac{D\pi r_0^2}{mq^2\Lambda_{eff}}c_0, \tag{33}$$

wherein $c_0 = c_{ent,0}$ denotes the concentration across the entrance of the trunk, consistent with the terminology of Eqn. 28 and $r_0 = r_{e_0}$ is the radius of the trunk. So, the effective exploration length, Λ_{eff} is a p, q–dependent expression,

$$\frac{\Lambda_{eff}}{L_0} = \frac{g_0}{q^2} \circ \frac{g_1}{q^2} \circ \cdots \circ \frac{g_n(\Lambda/L_0)}{q^2}, \tag{34}$$

wherein $L_0 = L_{e_0}$ is the length of the trunk. Equation 34 is the $n + 1$–fold functional composition of a branch-wise attenuating function $g_i = g_{e_i}$. This function itself is given by the formula

$$\frac{g_i(\Lambda/L_0)}{q^2} = \frac{(\Lambda/L_0)\,q^{-i/2}\phi_0 + \tanh\left[\left(p/\sqrt{q}\right)^i\phi_0\right]}{(\Lambda/L_0)\,q^{2-i}m\phi_0^2\tanh\left[\left(p/\sqrt{q}\right)^i\phi_0\right] + q^{2-i/2}m\phi_0}, \tag{35}$$

wherein $\phi_0 = L_0\sqrt{2/r_0\Lambda}$ is the Thiele modulus of the entrance branch, but depends on the exploration length penetrating into the tree.

4.2.4 Attenuating function as a Möbius transformation

Equation 35 is a Möbius transformation (Needham, 2007), and using this fact, Eqn. 34 can be expressed analytically. Möbius transformations, denoted by μ, are mappings that rotate, stretch, shrink, or invert curves on the complex plane, and take the following form (Needham, 2007): $\mu(z) = az + b/cz + d$, wherein a, b, c, d, and z are complex numbers. Remarkably, functional compositions of μ can also be calculated by multiplying matrices derived from it, termed Möbius matrices, drastically reducing the complexity of the functional-composition problem.

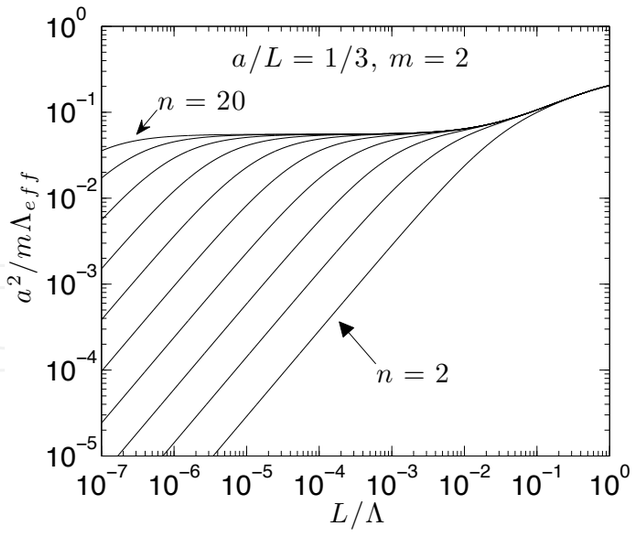

Fig. 6. Scaled currents as given by the square-channel model for trees of differing depth, n. Here, lengths are scaled in units of channel length, $L = 3a$.

Denoting the branch-wise Möbius matrix of g_i/q^2 by G_i, we construct

$$G_i = \begin{pmatrix} q^{-i/2}\phi_0 & \tanh\left[\left(p/\sqrt{q}\right)^i \phi_0\right] \\ q^{2-i}m\phi_0^2 \tanh\left[\left(p/\sqrt{q}\right)^i \phi_0\right] & q^{2-i/2}m\phi_0 \end{pmatrix}. \tag{36}$$

The effective exploration length, $\Lambda_{eff}/L_0 = D_{eff}/L_0 W_{eff}$, can be calculated according to

$$\prod_{i=0}^{n} G_i \begin{pmatrix} D/L_0 \\ W \end{pmatrix} = \begin{pmatrix} D_{eff}/L_0 \\ W_{eff} \end{pmatrix}. \tag{37}$$

In the special case of a "symmetric" tree, i.e. $p = q = 1$, the fully fractal Möbius matrix, Eqn. 37, reduces to

$$G_i = \begin{pmatrix} \phi_0 & \tanh\phi_0 \\ m\phi_0^2 \tanh\phi_0 & m\phi_0 \end{pmatrix}. \tag{38}$$

A fully analytical formula can be derived from this simplification by diagonalizing this 2×2 matrix, but this procedure and its implications will be presented elsewhere (Mayo et al., 2011).

Note that Eqns. 33 to 35 of the Cayley tree model, and Eqns. 27 and 28 of the square-channel model are predictions for the same quantity: the total current leaving the tree through its "reactive" side-walls. While the square-channel model is restricted to describe branches of equal width and length, the Cayley the model carries no such limitation. This scaling is quantified by inclusion of the trees' two fractal dimensions, D_{tree} and D_{canopy}, implied by the length and width ratios p and q, respectively.

Although the Cayley tree model is more general than the square-channel model in this respect, there are firm physiological data demonstrating the length and width of alveolar ducts remain constant with increasing generation in the human lung, i.e. $p = q = 1$ (Weibel, 1984), allowing for a direct comparison between the Cayley tree and square-channel models under application of this data to these models. The implications of the fracticality of the Cayley tree model will be discussed elsewhere.

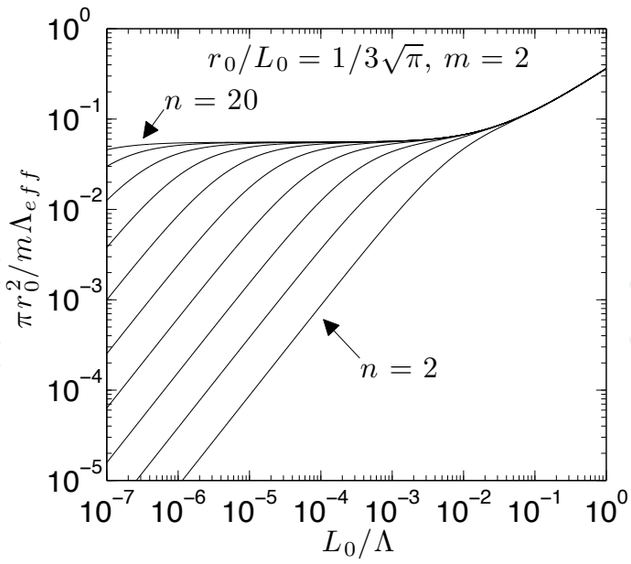

Fig. 7. Scaled currents given by the Cayley tree model for trees of varying depth, n. Here, r_0 and L_0 are the radius and length of the tree's entrance branch, respectively.

5. Reverse-engineering the robustness of mammalian lungs

5.1 Plateaus in the oxygen current associated with "robustness" to changing parameters

Despite differences in their geometrical treatment of the exchange surface, each of the models presented here (Rope-walk, square-channel, and Cayley tree models) predict the existence of a broad region in the exploration length, defined by $\partial I/\partial W = 0$, wherein the current entering the tree remains unchanged with respect to the surface's permeability.

Figure 6 illustrates this current, scaled in units of Dc_0 (fixed diffusivity), in the square-channel model. Here, L is the length of each channel, expressed in units of lattice constant a, and trees of differing depth, ranging from $n = 2$ to $n = 20$, in steps of two, are compared against one another. For smaller trees, the plateau is shorter, but the plateau is the largest for the larger trees (n or m large). Figure 7 illustrates the scaled current computed for the Cayley tree model. Plateaus similar to the square-channel model are presented, with the diameter of the source chosen by equating trunk cross-sectional areas with the square-channel model. Finally, figure 8 depicts currents computed using the Rope-Walk Algorithm, wherein the plateau widths are more clearly defined.

These plateaus describe a reduction in the active zones that is exactly matched by an increase in the permeability, or vice versa, keeping the current constant. Operation of mammalian lungs near the onset of these plateaus allows for the maximum current to be supplied to the blood by the lung while maintaining "robustness" necessary to mitigate any reduction in permeability that might occur from, for example, disease.

5.2 Screening regimes induced by diffusion of respiratory gases

These models each predict the existence of various screening regimes, which limit molecular access to the exchange area for different values of the surfaces' permeability. In the regime $\Lambda = 0$ ($W = \infty$), termed *complete screening* above, molecules do not explore further than the

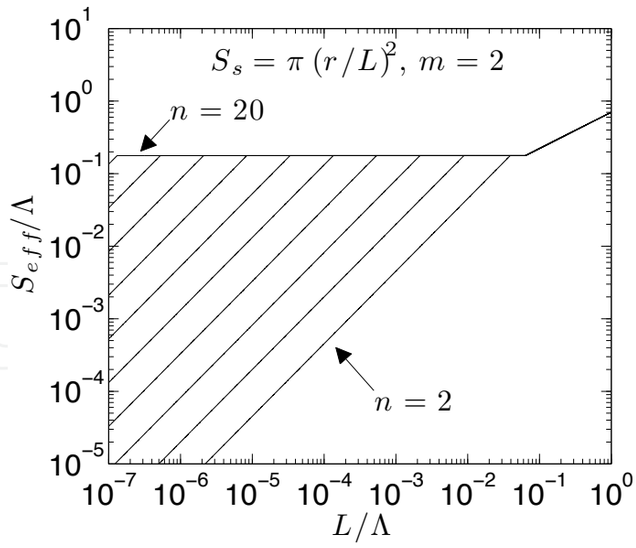

Fig. 8. Scaled currents in the Rope-Walk model for airway trees of varying size. Here, r and L denotes the radius and length of branches in the tree used to model the total gas-exchanger area.

entrance to the diffusion space, being absorbed by the exchange surface on their first contact with it. In the case of the Rope-Walk Algorithm model, this results in deep surface crevices possessing vanishing probability to admit any molecules. In both the Cayley tree and square channel models, this regime paints a picture in which vast amounts of surface area go unused, so that any effort in maintaining or creating the size and shape of the tree is wasted. In the opposite regime, $\Lambda = \infty$ ($W = 0$), the entire surface is visited by molecules, although they never cross it. Between these two extremes lies a region in which some, but not all, of the surface is explored. In this region, a balance between maximizing both the area of the active zones and the current crossing them guarantees that a minimum of the surface area is unused in the transport across it. Furthermore, direct validation of the partial screening regimes may be difficult, as the region of constant current cannot provide a unique value for the exploration length (or permeability) when measured under experimental conditions.

5.3 Efficiency of the gas-exchanger

The efficiency of the gas-exchanger, η_g, is defined as the ratio of current crossing the exchange surface to the total available current: $\eta_g = I/WS_g c_0 = S_{eff,g}/S_g$, giving a dimensionless measure of the gas-exchangers' performance, and can also be computed as the ratio of effective to total surface area (Hou, 2005; Grebenkov et al., 2005). Applied to the square-channel model, this efficiency is given by:

$$\eta_g = \frac{a^2}{mS_g}\left(\frac{\Lambda}{f^{n+1}(\Lambda)}\right). \tag{39}$$

wherein the total surface area of the square-channel tree is $S_g = 4a^2(l+1)\sum_{i=1}^{n} m^i + m^n a^2$. In the Cayley tree model, this efficiency is given by

$$\eta_g = \frac{\pi\rho^2}{mq^2 S_g}\left(\frac{\Lambda}{L_0\Lambda_{eff}}\right), \tag{40}$$

Parameter	Unit	Value			
		Rest	Moderate	Heavy	Maximum
Convection-diffusion transition	n/a	18	19	20	21
S_g	cm^2	6.75	3.36	1.69	0.844
N_g	$\times 10^5$	1.81	3.63	7.26	14.5
$c_a - c_b\beta_a/\beta_b$	$\times 10^{-7}$ moles/ml	1.97	4.10	4.97	4.51

Table 1. Data used for evaluating the mathematical models at varying levels of exercise, from ref. (Hou et al., 2010).

with the surface area of the fractal tree given by $S_g = 2\pi r_0 L_0 \sum_{i=0}^{n} (pqm)^i + (q^2 m)^n \pi r_0^2$ (Mayo, 2009). Finally, the efficiency of the Rope-Walk Algorithm is easily computed from Eqns. 14 by dividing them by the measured area of a gas exchanger, which serves as the area of the fractal surface across which the oxygen transport occurs.

To compute the current crossing the exchange surface in the human lung, the efficiency of a single gas exchanger is considered to be the same for all N_g–many gas-exchangers of the lung. This approximation gives:

$$I = N_g W \eta_g S_g \left(c_{air} - c_{blood}\beta_{air}/\beta_{air}\right), \tag{41}$$

wherein the values for the physiological parameters N_g, S_g, and $c_{air} - c_{blood}\beta_{air}/\beta_{blood}$ depend on the exercise state (Hou et al., 2010).

6. Validating these models against experimental data

The experimental data necessary to evaluate Eqn. 41 have been recently tabulated (Sapoval et al., 2005; Hou et al., 2010), from which exercise-independent parameters, valid for all models, are found. Here, the diameter of an single alveoli, $l_a = 0.0139$ cm (Hou et al., 2010), serves as the inner cut-off of the fractal surface in the Rope-Walk model, but is also taken as the smallest length scale in both the Cayley tree and square-channel models, i.e. $l_a = 2r_0$. Moreover, the permeability of the alveolar membranes to molecular oxygen, $W = 0.00739$ cm/sec (Hou et al., 2010), and its diffusivity of oxygen in air, $D_a = 0.243$ cm^2/sec (Hou et al., 2010), can be used to estimate the physiological value of the exploration length $\Lambda = D_a/W = 32.88$ cm. Finally, the Cayley tree and square-channel models must also include the length of their branches, taken in both models as the averaged length of an alveolar duct, $L_0 = 0.0736$ cm (Sapoval et al., 2005). Previous measurements firmly establish that the actual duct-length and -radius do not appreciably change with acinar branching generation (Haefeli-Bleuer & Weibel, 1988). In the Cayley tree model, this fact sets the branch-scaling parameters $p = q = 1$, corresponding to diverging fractal dimensions. The acinar tree, therefore, completely overfills the available space, packing the most exchange area into the pleural cavities in the fewest branching generations.

Exercise-dependent parameters are given in Table 1, tabulated from ref. (Hou et al., 2010) for all four exercise regimes considered here (rest, moderate, heavy, and maximum exercise). In the Rope-Walk model, these regimes conceptualize an increase in the active zones, resulting in the oxygen penetrating increasingly deeper crevices of the fractal surface. In the Cayley tree and square-channel models, these changing parameters associate with an oxygen source being pushed deeper into the tree, leaving a "smaller" gas-exchanger/subacinus for increasing

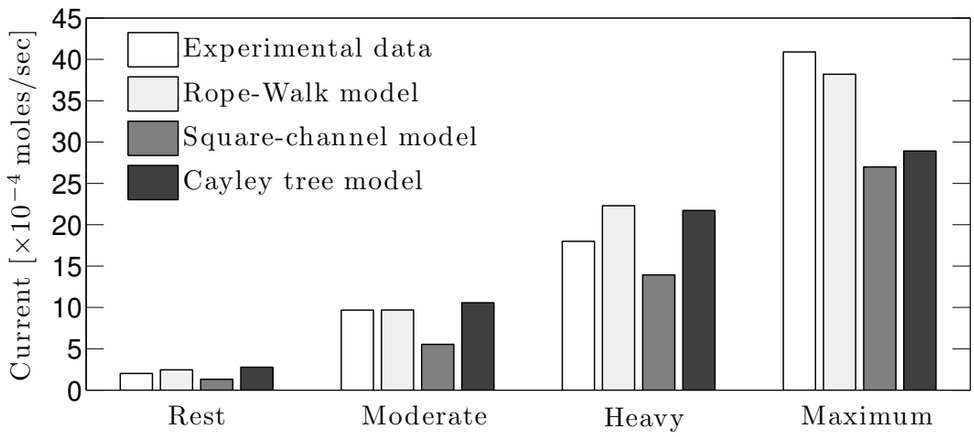

Fig. 9. Comparison between predicted values and the means of the measured oxygen uptake rates/currents at varying exercise levels.

exercise levels. This is reduction is balanced, however, with a drastic increase in the number of activated gas exchangers (Hou et al., 2010).

Figure 9 compares the predictions of these models to the measured currents for each exercise regime as reported by (Hou et al., 2010). Due to the discrete nature of the square-channel model, the length of a channel is restricted to be an integer multiple of its diameter (Grebenkov et al., 2005). So, setting $a = 0.0139$ cm requires that $l = 0.0760$ cm $/0.0139$ cm $= 5.47$; however, we rounded this value down to $l = 5$. Nevertheless, all models give reasonable agreement with the available data for the currents, with the Rope-Walk model giving closest agreement. This should be contrasted with the entirely different treelike models. We find the Cayley model to perform better than the square-channel model when equating their smallest length scales.

7. Industrial applications of lung-derived robustness

In this reverse engineering study, a finished product, the human lung, was deconstructed into its elementary processes/structures using mathematical modeling as the main investigative tool. Using this process, we uncovered a mechanism, termed diffusional screening, responsible for robustness of the prototypical lung studied here that functions by adjusting the area of the active zones in response to any loss of surface permeability, without any feedback loops or addition of any extra "hardware." Because aspects of some engineered processes evolve according to Eqns. 4 to 6, such as voltages, chemicals, or temperatures, they may also benefit from similar robustness derived, in part, from a treelike/fractal exchange surface. Here we briefly review just few examples.

7.1 Fuel cells

Fuel cells transduce chemical energy from a fuel (e.g. hydrogen, methane) into electrical energy through catalysis with an oxidizing agent (e.g. oxygen). Unfortunately, current devices lack the efficiency necessary to support wide-spread implementation in areas such as the transportation sector. Recent work, however, shows such efficiency can be improved 10-20% for a single cell of a stack-based setup using lung-inspired designs (Kjielstrup et al., 2010).

7.2 Heterogeneous catalysis

An active area of research in chemical engineering concerns the study of the chemical yield, and other properties, resulting from a gas or liquid reactant in contact with a solid nanoporous catalyst. It is known, for example, that the pore-size distribution influences the catalytic efficiency, wherein the reaction proceeds according to first-order kinetics (Gheorghui & Coppens, 2004). In this context Eqns. 4 to 6 describe the steady-state reactant concentration, while the total current, Eqn. 7, gives the yield. Although the resulting robustness of the lung's treelike "design" might protect against potential problems such as catalytic poisoning, it is not optimal in the sense of maximizing the reaction yield (Gheorghiu & Coppens, 2004).

7.3 Heat distribution systems

A nontrivial problem in thermal conduction is to efficiently distribute a localized heat source throughout a dissipation volume, preventing temperature increases at the source. Recent results from optimization analysis demonstrate the most efficient configuration of such a heat-transport network is treelike (Bejan, 2006). In many circumstances, temperature gradients evolve according to equations of the type in Eqns. 4 to 6, when heat is allowed to leak through the materials and into the environment (Carslaw & Jaeger, 1986). Results shown in Figs. 6 through 8 therefore equally describe heat transport across treelike and fractal surfaces, and suggest that treelike heat-pipe networks may be more tolerant to variations in material and manufacturing quality.

8. Conclusions

Although the partial pressure difference of oxygen in the gas-exchange regions of mammalian lungs increases only two-fold under the heaviest exercise conditions, the actual current increases approximately 20–fold, leaving another mechanism to supply the difference. Reverse engineering using mathematical modeling revealed that, depending on the exercise level, portions of the exchange surface of alveolar membranes remain "inactive" in any oxygen transport, so that a smaller effective area is responsible for supplying the oxygen current to the blood. With increasing exercise/breathing states, increasing surface areas are activated, drastically increasing the total oxygen uptake rate. This screening mechanism is termed "diffusional screening." Transitions between no- and partial-screening regimes mark a region in which the exploration length matches any decrease in the active zones due to oxygen inaccessibility to the exchange surface, establishing a broad plateau in the total current indicative of robustness. That is, altered diffusivity or permeability produces no change to the total current across several orders of magnitude, without the addition of any extra "hardware."

Other engineered systems, such as fuel cells, heterogeneous catalytic reactors, and heat pipes are described by the same fundamental processes: diffusion through a service volume and "reaction" along its surface. Using this information, structural designs of these industrial systems might be reengineered to mitigate the effects of uncertainties in manufacturing processes or material properties.

9. References

[1] Bejan, A., and Lorente, S. (2006). Constructal theory of generation of configuration in nature and engineering. *J. Appl. Phys.*, Vol. 100, pp. 041301.

[2] Carslaw, H.S., and Jaeger, J.C. (2000). *Conduction of Heat in Solids*, Oxford University Press Inc., New York, NY.
[3] Comroe, J.H. (1962). *The lung; clinical physiology and pulmonary function tests*, Year Book Medical Publishers, Chicago, IL.
[4] Felici, M. and Filoche, M. and Sapoval, B. (2003). Diffusional screening in the human pulmonary acinus. *J. Appl. Physiol.*, Vol. 94, pp. 2010.
[5] Felici, M. and Filoche, M. and Sapoval, B. (2004). Renormalized Random Walk Study of Oxygen Absorption in the Human Lung. *Phys. Rev. Lett.*, Vol. 92, pp.068101.
[6] Gheorghiu, S., and Coppens, M.-O. (2004). Optimal bimodal pore networks for heterogeneous catalysis. *AIChE J.*, Vol. 50, pp. 812.
[7] Grebenkov, D. S. and Filoche, M. and Sapoval, B. and Felici, M. (2005). Diffusion-Reaction in Branched Structures: Theory and Application to the Lung Acinus. *Phys. Rev. Lett.*, Vol. 94, pp. 050602.
[8] Haefeli-Bleuer, B., and Weibel, E.R. (1998). Morphometry of the human pulmonary acinus *Anat. Rec.*, Vol. 220, pp. 401.
[9] Hou, C. (2005). *Scaling laws for oxygen transport across the space-filling system of respiratory membranes in the human lung*, PhD thesis, University of Missouri, Columbia, MO.
[10] Hou, C., Gheorghiu, S., Huxley, V.H., and Pfeifer, P. (2010). Reverse Engineering of Oxygen Transport in the Lung: Adaptation to Changing Demands and Resources through Space-Filling Networks. *PLoS Comput. Biol.*, Vol. 6, No. 8, pp. e1000902.
[11] Kjelstrup, S., Coppens, M.-O., Pharoah, J.G., and Pfeifer, P. (2010). Nature-Inspired Energy- and Material-Efficient Design of a Polymer Electrolyte Membrane Fuel Cell. *Energy Fuels*, Vol. 24, pp. 5097.
[12] Mayo, M. (2009). *Hierarchical Model of Gas-Exchange within the Acinar Airways of the Human Lung*, PhD thesis, University of Missouri, Columbia, MO.
[13] Mayo, M. Gheorghiu, S., and Pfeifer, P. (2011). *Diffusional Screening in Treelike Spaces: an Exactly Solvable Diffusion-Reaction Model*, *Submitted*.
[14] Mandelbrot, B. (1982). *The Fractal Geometry of Nature*, W.H. Freeman, USA.
[15] Needham, T. (2007). *Visual Complex Analysis*, Oxford University Press, USA.
[16] Pfeifer, P., and Sapoval, B. (1995). Optimization of diffusive transport to irregular surfaces with low sticking probability. *Mat. Res. Soc. Symp. Proc.*, Vol. 366, pp. 271.
[17] Sapoval, B., Filoche, M., and Weibel, E.R. (2002). Smaller is better–but not too small: A physical scale for the design of the mammalian pulmonary acinus. *Proc. Natl. Acad. Sci. USA*, Vol. 99, No. 16, pp. 10411.
[18] Weibel, E.R. (1984). *The Pathway for Oxygen*, Harvard University Press, Cambridge, MA.
[19] Weibel, E.R., Taylor, C.R., and Hoppeler, H. (1992). Variations in function and design: Testing symmorphosis in the respiratory system. *PLoS Comp. Biol.*, Vol. 6, No. 8, pp. e1000902
[20] Weibel, E.R., Sapoval, B., and Filoche, M. (2005). Design of peripheral airways for efficient gas exchange. *Respir. Physiol. Neurobiol.*, Vol. 148, pp. 3.

Reverse Engineering - Recent Advances and Applications

Edited by Dr. A.C. Telea

ISBN 978-953-51-0158-1

Hard cover, 276 pages

Publisher InTech

Published online 07, March, 2012

Published in print edition March, 2012

Reverse engineering encompasses a wide spectrum of activities aimed at extracting information on the function, structure, and behavior of man-made or natural artifacts. Increases in data sources, processing power, and improved data mining and processing algorithms have opened new fields of application for reverse engineering. In this book, we present twelve applications of reverse engineering in the software engineering, shape engineering, and medical and life sciences application domains. The book can serve as a guideline to practitioners in the above fields to the state-of-the-art in reverse engineering techniques, tools, and use-cases, as well as an overview of open challenges for reverse engineering researchers.

How to reference

In order to correctly reference this scholarly work, feel free to copy and paste the following:

Michael Mayo, Peter Pfeifer and Chen Hou (2012). Reverse-Engineering the Robustness of Mammalian Lungs, Reverse Engineering - Recent Advances and Applications, Dr. A.C. Telea (Ed.), ISBN: 978-953-51-0158-1, InTech, Available from: http://www.intechopen.com/books/reverse-engineering-recent-advances-and-applications/reverse-engineering-the-robustness-of-mammalian-lung

INTECH
open science | open minds

InTech Europe
University Campus STeP Ri
Slavka Krautzeka 83/A
51000 Rijeka, Croatia
Phone: +385 (51) 770 447
Fax: +385 (51) 686 166
www.intechopen.com

InTech China
Unit 405, Office Block, Hotel Equatorial Shanghai
No.65, Yan An Road (West), Shanghai, 200040, China
中国上海市延安西路65号上海国际贵都大饭店办公楼405单元
Phone: +86-21-62489820
Fax: +86-21-62489821